Journal of Alloys and Compounds 513 (2012) 75–79

Contents lists available at SciVerse ScienceDirect

Journal of Alloys and Compounds

journal homepage: www.elsevier.com/locate/jallcom

Microstructure evolution of $Zr_{65}Al_{7.5}Cu_{12.5}Ni_{10}Ag_5$ bulk metallic glass due to rolling and its influence on the thermal stability

Z.J. Yan*, J. Yan, Y. Hu, W.X. Hao

School of Materials Science and Engineering, Taiyuan University of Science and Technology, Taiyuan 030024, PR China

ARTICLE INFO

Article history:
Received 26 June 2011
Received in revised form 2 September 2011
Accepted 3 September 2011
Available online 5 October 2011

Keywords:
Metallic glasses
Phase transitions
Kinetics
Icosahedral phase

ABSTRACT

X-ray diffraction (XRD), differential scanning calorimetry (DSC) and high-resolution transmission electron microscopy (HRTEM) are employed to investigate the microstructure evolution of $Zr_{65}Al_{7.5}Cu_{12.5}Ni_{10}Ag_5$ bulk metallic glass subjected to rolling at room temperature. The strain rates are controlled to be 10^{-4}–10^{-3} s^{-1}. The results show that the plastic deformation during rolling behaves as an inhomogeneous mode with the characteristic of shear bands, which results in the two-state characteristic of atomic movement from competition between the ordering and disordering processes. The icosahedron-like clusters precipitate in the transition regions between the shear bands and the amorphous matrix, and they tend to aggregate into nano-sized orders. The results of DSC indicate that the onset precipitation temperature of I-phase during heating of the metallic glass obviously decreases due to rolling. However, the time window for the completion of amorphous-to-icosahedral phase transformation is evidently lengthened. The microstructure evolution during rolling and its influence on the thermal stability are discussed.

1. Introduction

Metallic glasses (MGs) are thermodynamically metastable, and they tend to crystallize upon heating [1]. Due to excellent mechanical properties and superplasticity in supercooled liquid region [2,3], MGs are of great technical and academic interests. Much progress has been achieved in the preparation, thermal stability and mechanical properties of MGs in recent decades [4]. It has been reported that icosahedral phase (I-phase) precipitates as the primary phase during heating of the $Zr_{65}Al_{7.5}Cu_{12.5}Ni_{10}Ag_5$ MG [5]. The structural unit of I-phase is one showing a rotational but not translational order [6], which is metastable and tends to decompose into a more stable state. It has been found that I-phase precipitates in Al-, Mg-, Zr- and Ti-based alloys [7,8]. Köster et al. have found that I-phase forms during devitrification of Zr–Cu–Al and Zr–Cu–Ni–Al MGs [9], which does not occur in Inoue's work [10]. The previous works indicate that the formation of I-phase is sensitive to the noble metals (e.g., Ag, Pb, Au, Pt) and oxygen content [11–13].

It has been revealed that shear flow induces nanocrystallization in a MG during plastic deformation, which is different from the crystallization due to heating [14,15]. It has been found that the effective activation energies for crystallization during heating of the $Fe_{65}Ni_{17}Si_7B_{11}$ and $Fe_{72}Co_8Si_8B_{12}$ MGs are 1.8 eV and 2.2 eV, respectively, but the latter shows more stable during milling [16]. This suggests that the mechanical stability of a MG is obviously different from its thermal stability. Investigating the microstructure evolution during plastic deformation of a MG, in which metastable phase precipitates upon heating, is an alternative method to understand the mechanical stability of a MG. Recently, we have found that tetragonal micrometer-sized $CuZr_2$ or (and) $NiZr_2$ crystals precipitate under the indenter edges during Vickers indentation of the $Zr_{65}Al_{7.5}Cu_{12.5}Ni_{10}Ag_5$ MG [17], indicating the formation of metastable I-phase is depressed. The depth of a Vickers indent is estimated to be about 6 μm, which is much higher than the typical thickness (about 80–100 nm) for TEM observation. As a result, a whole morphology of a Vickers indent in the TEM observation is impossible. As an often-used method to produce severe plastic deformation, rolling can exclude the uncertainty in strain rate and the temperature rise. Furthermore, morphology and microstructures of the shear bands during rolling can be directly observed in TEM images. In the previous works, we have observed nanocrystals with size about 5–10 nm on the transition regions between the shear bands and the amorphous matrix in the $Zr_{60}Al_{15}Ni_{25}$ MG subjected to rolling at room temperature [18]. Based on the background above, the microstructure evolution of the $Zr_{65}Al_{7.5}Cu_{12.5}Ni_{10}Ag_5$ MG during rolling at room temperature is investigated in the present work to attempt to understand the mechanical stability of a MG and its relation with the thermal stability.

2. Experimental

An ingot of nominal composition of $Zr_{65}Al_{7.5}Cu_{12.5}Ni_{10}Ag_5$ (atomic percent) was prepared by arc melting the mixture of pure metals Zr, Al, Ni, Cu, and Ag (99.9 wt%)

* Corresponding author. Tel.: +86 351 6998256; fax: +86 351 6998256.
E-mail address: yanzhijie74@sohu.com (Z.J. Yan).

0925-8388/$ – see front matter © 2011 Elsevier B.V. All rights reserved.
doi:10.1016/j.jallcom.2011.09.083

Table 1
Detailed DSC data of the as-cast and some rolled specimens at the heating rate of 20 K/min.

ε (%)	T_x (K)	T_e (K)	$\Delta T = T_e - T_x$ (K)	ΔH (J/g K)
0	716.0	742.8	26.8	30.2
40	713.4	742.4	29.0	30.2
80	713.6	742.7	29.1	30.1
95	710.0	742.1	32.1	30.2

in a water-cooled copper crucible under titanium-gettered high purity argon atmosphere. The ingot was remelted 4 times to ensure its compositional homogeneity. Specimens with a cross-section of 1 mm × 10 mm and length about 50 mm were produced from the ingot by suction casting in a copper mold.

Amorphous nature of the as-cast specimens was identified by X-ray diffraction (XRD, RIGAKU/max-Ra) using Cu K_α radiation. These as-cast specimens were cut into small bars with a cross-section of 1 mm × 2 mm and length of 10 mm for subsequent rolling. These bars, covered by two steel foils, were rolled at room temperature to the desired thickness in a twin-roller apparatus with a roll diameter of 120 mm. The deformation was carefully controlled to ensure the strain rates to be 10^{-4}–10^{-3} s^{-1}. The deformation degree (ε) was evaluated by the reduction in thickness, i.e., $\varepsilon = (h_0 - h)/h_0$, where h_0 and h stood for the specimen thickness of as-cast and as-rolled specimens, respectively. The maximum ε of 95% was obtained in the present work.

Thermal analyses were performed in a Perkin-Elmer Pyris Diamond differential scanning calorimeter (DSC) at a scanning rate of 20 K/min under flow of high purity argon. The microstructures of the rolled $Zr_{65}Al_{7.5}Cu_{12.5}Ni_{10}Ag_5$ specimens were investigated by XRD and high-resolution transmission electron microscopy (HRTEM, JEOL JEM-2100 F) under an accelerating voltage of 200 kV. The TEM foils with a diameter of 3 mm were prepared using a twin-jet thinning electropolisher in a solution of 5% (volume percent) perchloric acid and 95% ethanol at 243 K. The energy disperse spectrum (EDS) was employed to investigate the distribution of the elements on the regions of shear bands and the transition regions between the shear bands and the undeformed matrix. The average value based on three EDS tests was evaluated to present the composition on one region.

3. Results and discussion

The XRD patterns of as-cast and some rolled specimens are shown in Fig. 1(a). Besides the broad diffraction peaks, no obvious sharp peaks were detected in these XRD patterns, which indicates that no quasicrystals or crystals are detected within the sensitivity of XRD technique. It is verified that the as-cast alloy is amorphous. By fitting the broad diffraction peaks located at $2\theta \approx 37^\circ$ in the XRD patterns using Lorentz line profiles, the values of full width at the half maximum (FWHM) are evaluated and shown in Fig. 1(b). It is obvious that the variation of FWHM with ε is not monotonic. The value of FWHM decreases from 4.2° to 3.8° with increase of ε from 0% (as-cast) to 10%, and it increases within ε = 10–30%. The variation of value of FWHM with ε shows a saddle-like tendency as ε = 30–95%, showing the maximum value of 4.5° at ε = 70%. The larger value of FWHM means a more disordered atomic configuration. The non-monotonic variation of value of FWHM with ε suggests a two-state characteristic of atomic movement resulting from the competition between ordering and disordering processes, which agrees with our previous work in the $Zr_{60}Al_{15}Ni_{25}$ MG [19].

Fig. 2 shows the DSC curves of the as-cast and some rolled specimens recorded at the scanning rate of 20 K/min. All the DSC traces show three exothermic events corresponding to the crystallization processes. Our previous work indicates that the first exothermic process is due to the precipitation of icosahedral phase (I-phase) based on the XRD pattern (not shown here) [5]. And at higher temperature, the residual amorphous phase and I-phase begin to decompose into more stable phases $CuZr_2$ and (or) $NiZr_2$ [5]. The detailed DSC data are shown in Table 1. The onset precipitation temperature (T_x) of I-phase decreases due to rolling, e.g., the value of T_x decreases about 6 K with increase of ε from 0% to 95%, which indicates that the formation of I-phase is more easily triggered due to rolling. There are no obvious changes of the end crystallization temperature (T_e) and the exothermic enthalpy (ΔH) of the first exothermic peak, but the width of exothermic peak

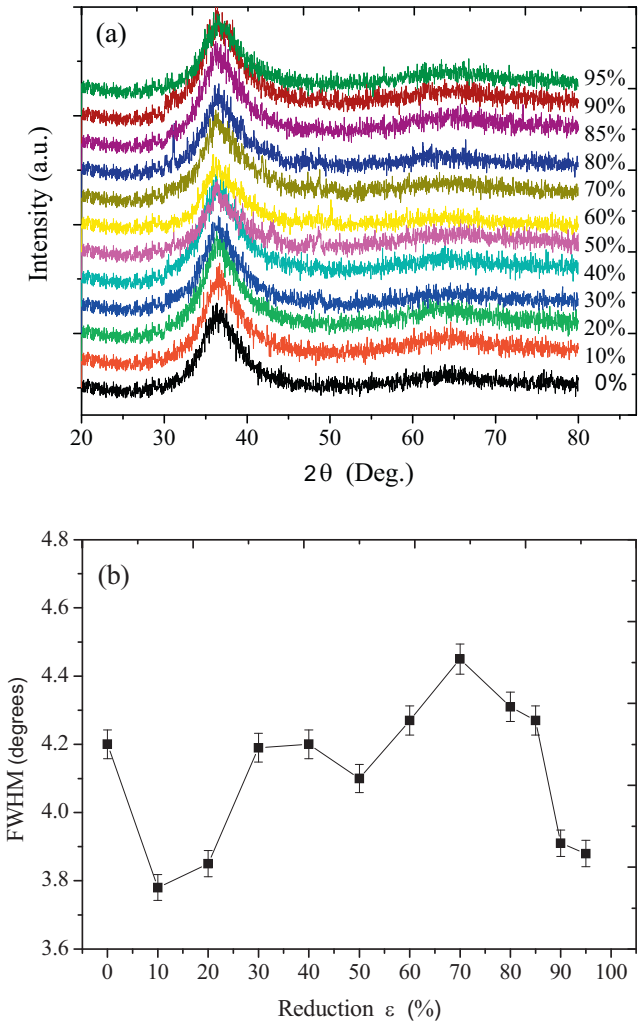

Fig. 1. XRD patterns of the as-cast and some rolled specimens (a), and the corresponding FWHM values of the main diffraction peaks obtained from Lorentz fitting (b).

($\Delta T = T_e - T_x$) obviously increases. These DSC data indicate that the volume fraction of precipitated I-phase during heating nearly keeps identical, but the time window for the amorphous-to-icosaheral phase transformation obviously becomes longer due to rolling. This phenomenon can be explained by the microstructure changes due to rolling.

In the HRTEM images, there appear white bands, i.e., shear bands (Figs. 3–5), indicating an inhomogeneous plastic

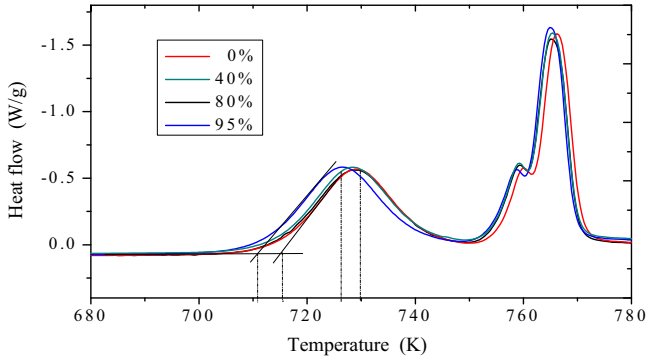

Fig. 2. DSC traces of the as-cast and some rolled specimens at the heating rate of 20 K/min.

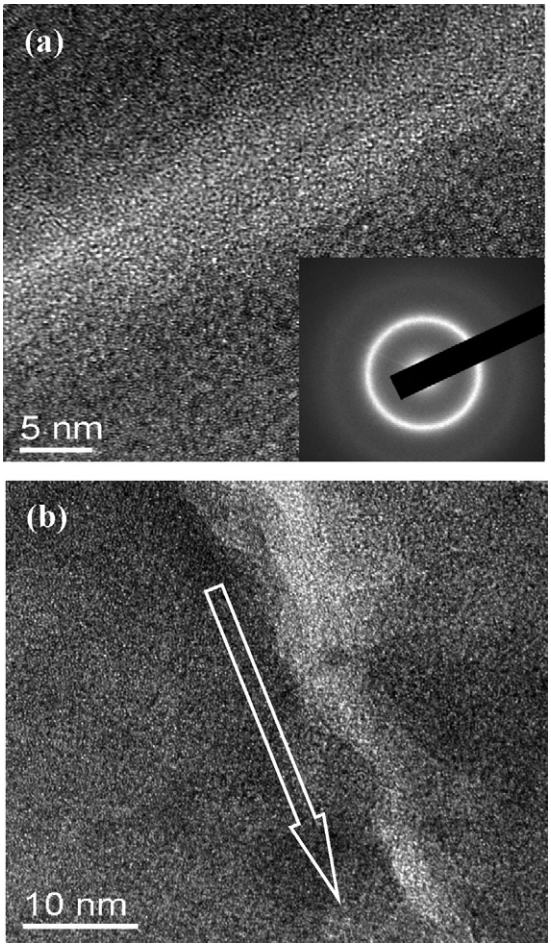

Fig. 3. HRTEM images of the rolled specimens of $\varepsilon = 20\%$ (a) and $\varepsilon = 40\%$ (b), the inset in (a) is the SAED pattern of the shear band.

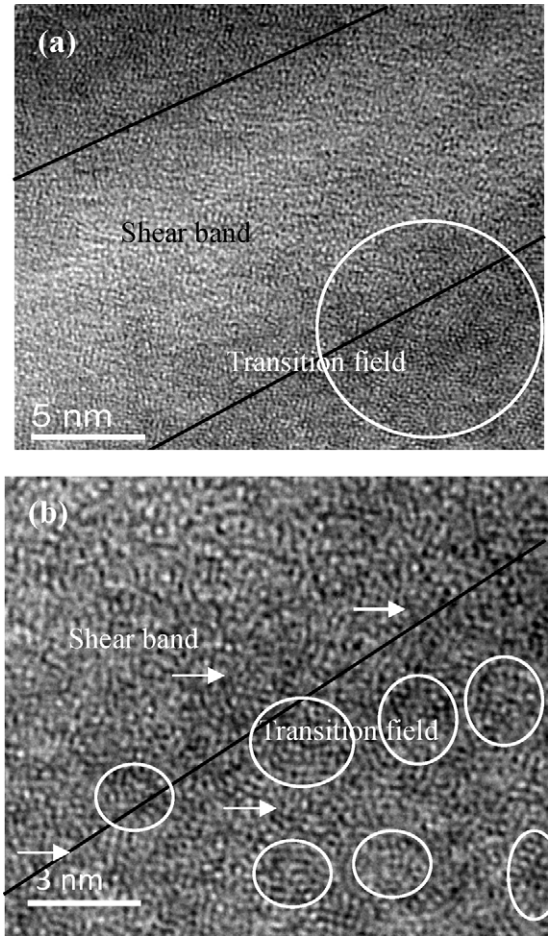

Fig. 4. HRTEM image of one shear band in the specimen of $\varepsilon = 80\%$ (a), and the magnified image of the circled region (b).

deformation during rolling at room temperature. The plastic deformation localizes in these shear bands, during which shear stress induces shear transformation events and results in the shear dilatation with the characteristic of viscous flow, and therefore, introduction of more excess free volume [20]. These shear bands appear as bright regions since they are thinner than the undeformed matrix due to less resistance to chemical attack during thinning [21]. Fig. 3(a) shows the HRTEM image of the specimen of $\varepsilon = 20\%$, showing the shear bands with size about 20 nm. The inset is the selected area electron diffraction (SAED) pattern of one shear band, indicating long-range disordered atomic configuration. The HRTEM image of the specimen of $\varepsilon = 40\%$ is shown in Fig. 3(b). It indicates that the plastic deformation regions develop with further rolling, which results in more excess free volume, suggesting a more disordered atomic configuration.

Fig. 4(a) shows the HRTEM image of one shear band in the rolled specimen of $\varepsilon = 80\%$, and the magnified image of the circled region is shown in Fig. 4(b), indicating formation of many clusters. During rolling, the introduction of excess free volume in the shear bands results in a state with higher energy, under which the driving force for phase transformation increases. These clusters aggregate into short-range orders (which are too small to be called as crystals) during rolling, which results in an ordering process to release the accumulated excess energy [22]. On the other hand, the excess free volume coalesces into nanovoids to relax the instability of atomic configuration [23]. The ordering process and coalescence of excess free volume lead to formation of short-range orders (or clusters) (Fig. 4). Based on the configuration characteristics, these clusters are icosahedron-like ones. Theoretically, the direct characterization of the atomic configuration of these orders (clusters) is the SAED patterns. In the present work, the orders are too small to be identified by SAED technique even if under nanobeam. The atomic characteristic of these orders is indirectly identified by the DSC data, which is discussed later.

Fig. 5(a) shows a HRTEM image of one shear band in the rolled specimen of $\varepsilon = 95\%$, and the marked rectangle region is magnified in Fig. 5(b). It is obvious that more clusters form in the specimen of $\varepsilon = 95\%$ than in the one of $\varepsilon = 40\%$. Based on the HRTEM images, it is clear that no crystals or quasicrystals precipitate in the rolled specimens. However, the atomic configuration in the deformed region obviously changes, forming icosahedron-like orders. Based on the free volume model [24], the creation of free volume accompanies with annihilation of free volume during plastic deformation. At the initial stage, the creation rate of free volume is much higher than that of annihilation. As a result, more excess free volume introduces in the deformed region, meaning a more disordered atomic configuration. With increase of deformation degree, the annihilation rate of free volume is larger than that of creation, resulting in formation of short-range orders. Fig. 6 shows the SEAD patterns of the specimens of $\varepsilon = 20\%$, 80% and 95%. The diffraction halo of $\varepsilon = 80\%$ is more dispersed than that of $\varepsilon = 20\%$ and 95%, suggesting that the atomic configuration of $\varepsilon = 80\%$ is more disordered than that of $\varepsilon = 20\%$ and 95%. This agrees with the results of FWHM. The competition between the creation and annihilation of excess free volume results in the two-state characteristic of atomic movement during rolling (Fig. 1(b)).

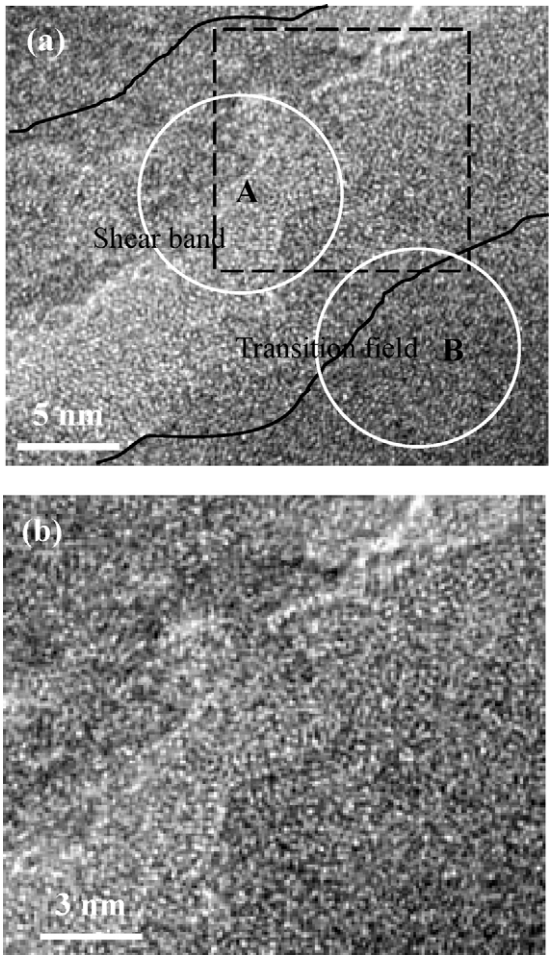

Fig. 5. HRTEM image of one shear band in rolled specimen of $\varepsilon = 95\%$ (a) and the magnified image of the marked rectangle region (b).

The results of energy disperse spectrum (EDS) in the shear bands, and the transition regions between the shear bands and the undeformed matrix, and the amorphous matrix in the specimen of $\varepsilon = 95\%$ are shown in Table 2. It indicates that the contents of Zr and Ag in the shear bands are lower than that in the transition regions and the matrix, but the contents of Al, Cu and Ni are higher. This suggests occurrence of atomic redistribution in the deformed regions. It has been found that Ag is favorable for precipitation of I-phase during crystallization of the Zr–Al–Cu–Ni–Ag MGs, and that quasicrystals with size about 20 nm productively precipitate as the content of Ag reaches 10 at% [9], indicating that Ag enhances formation of icosahedral clusters. With respect to the nominal content, the decrease of Ag in the shear bands depresses the formation of icosahedral clusters. In the transition regions between the shear bands and the undeformed matrix, the content of Ag is about 5.67%, which is higher than that in the shear bands and is expected to enhance the formation of icosahedral clusters. These clusters gradually aggregate into icosahedron-like short-range orders (Figs. 4 and 5). During heating of the rolled specimen, these short-range orders grow into I-phase as the pre-existing nuclei, which results in decrease of T_x (Table 1). The atomic movement in the deformed regions induced by shear flow is predominated by the propagation orientation of the shear bands [25], during which the atomic movement probability along the propagation direction of the shear bands is much higher than other directions. This leads to the inhomogeneous distribution of atoms in the deformed spaces. As a result, the redistribution of atoms for formation of icosahedral clusters becomes more difficult in the rolled specimen since the atomic movement probability in the 3-dimensional space is identical during heating. Therefore, the growth rate of I-phase becomes more sluggish in the rolled specimens, and the precipitation of I-phase completes in a wider temperature window (Table 1).

Table 2
Compositions in different regions of the rolled specimen of $\varepsilon = 95\%$ with errors of ±0.1 at%.

Regions	Zr (at%)	Al (at%)	Cu (at%)	Ni (at%)	Ag (at%)
Shear band	49.3	10.1	18.4	18.6	3.6
Transition region	55.6	9.0	16.3	14.3	5.7
Amorphous matrix	56.4	4.2	16.1	17.7	4.9

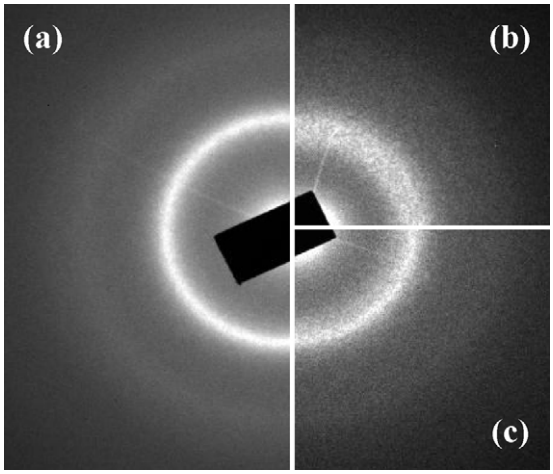

Fig. 6. SAED patterns of shear bands in the specimens of $\varepsilon = 20\%$ (a), 80% (b), and 95% (c).

4. Conclusions

The HRTEM images show that an inhomogeneous plastic deformation occurs during rolling of the $Zr_{65}Al_{7.5}Cu_{12.5}Ni_{10}Ag_5$ MG at room temperature. In the transition regions between the shear bands and the undeformed amorphous matrix, there form icosahedron-like clusters and these clusters aggregate into short-range orders. During the subsequent heating, these icosahedron-like orders grow as the pre-existing nuclei, which results in decrease of the onset precipitation temperature of I-phase during heating. The viscous flow leads to obvious redistribution of atoms in the shear bands, during which the atomic movement is predominated by the propagation direction of the shear bands, leading to the inhomogeneous distribution of atoms in the deformed spaces. Under this condition, the homogeneous redistribution of atoms during heating becomes more difficult in the deformed regions. As a result, the growth rate of I-phase becomes more sluggish, and the precipitation of I-phase completes in a wider time window.

Acknowledgements

This project was financially supported by the National Natural Science Foundation of China (Grant No. 50804032), the Natural Science Foundation of Shanxi Province, China (Grant No. 2011021020-1), and Program for Excellent Talents of Shanxi Province, China (2010).

References

[1] A. Inoue, Acta Mater. 48 (2000) 279.
[2] W.L. Johnson, Mater. Res. Bull. 24 (1999) 42.

[3] C.A. Schuh, T.C. Hufnagel, U. Ramamurty, Acta Mater. 55 (2007) 4067.
[4] Z.J. Yan, S.R. He, J.F. Li, Y.H. Zhou, J. Mater. Sci. 39 (2004) 5743.
[5] Z.J. Yan, J.F. Li, S.R. He, H.H. Wang, Y.H. Zhou, Mater. Trans. 44 (2003) 907.
[6] P.J. Steinhardt, S. Ostlund, The Physics of Quasicrystals, Word Scientific, Singapore, 1987.
[7] D. Shechtman, I. Blech, D. Gratias, J.W. Chan, Phys. Rev. Lett. 53 (1984) 1951.
[8] M.W. Chen, A. Inoue, T. Zhang, A. Sakai, T. Sakurai, Philos. Mag. Lett. 80 (2000) 263.
[9] U. Köster, J. Miehhardt, S. Roos, H. Liebertz, Appl. Phys. Lett. 69 (1996) 179.
[10] A. Inoue, D. Kawase, A.P. Tasia, T. Zhang, T. Masumeto, Mater. Sci. Eng. A 178 (1994) 255.
[11] M.W. Chen, T. Zhang, A. Inoue, A. Sakai, T. Sakurai, Appl. Phys. Lett. 75 (1999) 1697.
[12] A. Inoue, T. Zhang, J. Saida, M. Matsushita, M.W. Chen, T. Sakurai, Mater. Trans. JIM 40 (1999) 1181.
[13] A. Inoue, T. Zhang, J. Saida, M. Matsushita, M.W. Chen, T. Sakurai, Mater. Trans. JIM 40 (1999) 1137.
[14] Y. He, G.J. Shiflet, S.J. Poon, Acta Metall. Mater. 43 (1995) 83.
[15] H. Chen, Y. He, G.J. Shiflet, S.J. Poon, Nature (London) 367 (1994) 541.
[16] M.L. Trudeau, R. Schulz, D. Dussault, A. Van Neste, Phys. Rev. Lett. 64 (1990) 99.
[17] Z.J. Yan, J.F. Li, Y.H. Zhou, Y.Q. Wu, Acta Phys. Sin. 56 (2007) 999.
[18] Z.J. Yan, J. Yan, Y. Hu, S.E. Dang, Sci. China, Ser. E: Technol. Sci. 53 (2010) 278.
[19] Z.J. Yan, J.F. Li, Y.H. Zhou, Y.Q. Wu, Sci. China, Ser. E: Technol. Sci. 49 (2006) 655.
[20] B.P. Kanungo, M.J. Lambert, K.M. Flores, Mater. Res. Soc. Symp. 806 (2004) 295.
[21] Q.P. Cao, J.F. Li, Y. Hu, A. Horsewell, J.Z. Jiang, Y.H. Zhou, Mater. Sci. Eng. A 457 (2007) 94.
[22] G.W. Koebrugge, A. van den Beukel, Scripta Metall. 22 (1988) 589.
[23] W.J. Wright, T.C. Hufnagel, W.D. Nix, J. Appl. Phys. 93 (2003) 1432.
[24] F. Spaepen, Acta Metall. 25 (1977) 407.
[25] Y. Zhang, A.L. Greer, Appl. Phys. Lett. 89 (2006) 071907.